

Spin-Orbit Locked Coupling of Localized Microwaves to Magnons

Chengyuan Cai,^{1,*} Zubiao Zhang,^{1,*} Ji Zou,² Gerrit E. W. Bauer,^{3,4} and Tao Yu^{1,†}

¹*School of Physics, Huazhong University of Science and Technology, Wuhan 430074, China*

²*Department of Physics, University of Basel, Klingelbergstrasse 82, 4056 Basel, Switzerland*

³*WPI-AIMR and Institute for Materials Research and CSRN, Tohoku University, Sendai 980-8577, Japan*

⁴*Kavli Institute for Theoretical Sciences, University of the Chinese Academy of Sciences, Beijing 100190, China*
(Dated: June 5, 2024)

We address the photonic spin-orbit coupling known from nano-optics and plasmonics in the microwave regime. The transverse spin \mathbf{S} and momentum \mathbf{q} of microwaves emitted by an excited magnetic dot are locked by $\mathbf{q} \cdot \mathbf{S} = 0$ with a fixed chirality $\hat{\mathbf{n}} \cdot (\hat{\mathbf{S}} \times \hat{\mathbf{q}}) = 1$ when evanescent along $\hat{\mathbf{n}} \perp \mathbf{q}$. This field excites magnons in a nearby magnetic film in the form of directional beams that rotate with the magnetization direction. The exchange of these magnons through a magnetic substrate leads to a highly tunable strong coupling and entanglement between two distant nanomagnets.

Introduction.—Photonic spin-orbit coupling (SOC) in nano-optics [1–3] and plasmonics [4, 5] refers to the locking of photon “spin” and wave vector that allows unidirectional routing of photons and the photon quantum spin Hall effect.

Magnonics is a different field aiming for the excitation, detection, and control of magnons, the quanta of spin wave excitations of magnetic order [6–12], generating memory functionality and logic circuits [13, 14]. Magnons emit stray magnetic fields from gigahertz to terahertz that may excite microwave waveguides and interact with metals, superconductors, NV-centers in diamond, and other magnets. Single magnons can be generated and manipulated by the coupling to superconducting qubits [15–18]. Magnons at surfaces of bulk magnets [19, 20] and their stray fields in thin films [21] are chiral in the sense that their propagation normal to the magnetization is unidirectional, facilitating directional control of classical and quantum information flow [22]. Mediated by magnetic stray fields magnons couple chirally with photons [23–29], other magnons [30–37], electrons [38], Cooper pairs [39, 40], phonons [41–46], and qubits [47]. However, theoretical [23, 27, 28, 30, 37–39, 41, 47] and experimental [24–26, 29, 31–35, 40, 42–46] studies of magnon chirality have been limited to one-dimensional systems.

In this Letter, we unify the notion of photonic SOC at optical frequencies with the chiral coupling of magnets in the gigahertz regime. To this end, we demonstrate that the spin \mathbf{S} and momentum \mathbf{q} locked ac stray magnetic fields emitted by a point-like source in two dimensions results in a photonic (Rashba-like) SOC $\mathbf{q} \cdot \mathbf{S} = 0$ with chirality index $\hat{\mathbf{n}} \cdot (\hat{\mathbf{S}} \times \hat{\mathbf{q}}) = 1$ (see Fig. 1). Here hats indicate unit vectors and the field is evanescent normal to the plane of propagation $\hat{\mathbf{n}} \perp \mathbf{q}$. The effect allows the routing of magnons in extended ferromagnetic films by nanomagnets under ferromagnetic resonance (FMR). The directional coupling between two nanomagnets on a magnetic substrate by the exchange of film magnons can be tuned by the equilibrium magnetization directions and route magnon entanglement [48, 49]. The on-chip distant

entanglement does not require structuring the films and the associated deterioration of the magnetic quality.

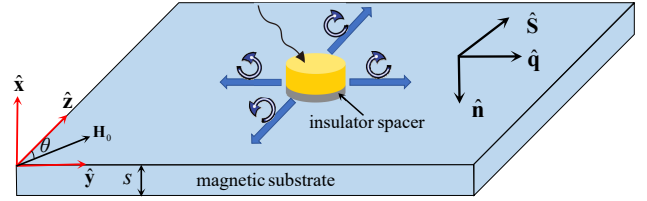


FIG. 1. Locking of microwave spin \mathbf{S} (curled arrows) and momentum \mathbf{q} (blue arrows) of the dynamic stray fields of a magnetic dot, governed by the chirality index $\hat{\mathbf{n}} \cdot (\hat{\mathbf{S}} \times \hat{\mathbf{q}}) = 1$ that excites a nearby magnetic film of thickness s into preferred directions. The stray field is evanescent along the normal $\hat{\mathbf{n}}$ and the hats indicate unit vectors.

Fixed chirality of evanescent vector fields.—A fundamental property of a vector field $\mathbf{V}(\mathbf{r}, t)$ is its angular momentum (or spin) distribution $\mathbf{S}(\mathbf{r}, t) \propto \text{Im}(\mathbf{V}^* \times \mathbf{V})$ [4, 21]. The angular momentum of an electromagnetic, i.e. electric \mathbf{E} and magnetic \mathbf{H} field, is $\mathbf{S} = 1/(4\Omega)\text{Im}(\varepsilon_0\mathbf{E}^* \times \mathbf{E} + \mu_0\mathbf{H}^* \times \mathbf{H})$ in vacuum, where Ω is the frequency and μ_0/ε_0 is the vacuum permeability/permittivity. The spin of a Fourier component \mathbf{q} is “transverse” (“longitudinal”) when $\mathbf{S} \perp \mathbf{q}$ ($\mathbf{S} \parallel \mathbf{q}$). Here we focus on the transverse spin of plane wave modes that propagate in two dimensions but are evanescent along the third field decay direction $\hat{\mathbf{n}}$. We measure the chirality by the index $\mathcal{C}_{\mathbf{q}} = \hat{\mathbf{n}} \cdot (\hat{\mathbf{S}} \times \hat{\mathbf{q}})$ [4, 21], which is “right-handed” when $0 < \mathcal{C}_{\mathbf{q}} \leq 1$, and “left-handed” when $-1 \leq \mathcal{C}_{\mathbf{q}} < 0$. According to the Helmholtz theorem, any vector field can be decomposed into rotation- and divergence-free components. When there are no sources the field is purely rotational.

We focus on an evanescent vector field $\mathbf{V}(\mathbf{r}, t) = \mathcal{V}e^{i(q_y y + q_z z) + \sqrt{q_y^2 + q_z^2}x} e^{-i\Omega t}$ in the negative half-space $x < 0$ that propagates in the y - z plane with wave vector $\mathbf{q} = q_y \hat{\mathbf{y}} + q_z \hat{\mathbf{z}}$ and frequency Ω , where the amplitudes are normalized as $\mathcal{V} = (1, \mathcal{V}_y e^{i\phi_y}, \mathcal{V}_z e^{i\phi_z})$ with $\text{Im}\mathcal{V}_{y,z} = 0$ and phases $\{\phi_y, \phi_z\} \in [0, 2\pi)$. In the absence of sources

$\nabla \cdot \mathbf{V}(\mathbf{r}, t) = 0$ or

$$\begin{aligned} q_y \mathcal{V}_y \cos \phi_y + q_z \mathcal{V}_z \cos \phi_z &= 0, \\ q_y \mathcal{V}_y \sin \phi_y + q_z \mathcal{V}_z \sin \phi_z &= \sqrt{q_y^2 + q_z^2}. \end{aligned} \quad (1)$$

The spin $\mathbf{S}(\mathbf{r}, t) \propto \text{Im} [\mathbf{V}(\mathbf{r}, t)^* \times \mathbf{V}(\mathbf{r}, t)]$ has the components [4]

$$\begin{aligned} S_x(x, q_y, q_z) &\propto -2\mathcal{V}_y \mathcal{V}_z \sin(\phi_y - \phi_z) e^{2\sqrt{q_y^2 + q_z^2}x}, \\ S_y(x, q_y, q_z) &\propto -2\mathcal{V}_z \sin \phi_z e^{2\sqrt{q_y^2 + q_z^2}x}, \\ S_z(x, q_y, q_z) &\propto 2\mathcal{V}_y \sin \phi_y e^{2\sqrt{q_y^2 + q_z^2}x}. \end{aligned} \quad (2)$$

Focusing on transverse vector fields

$$\mathbf{q} \cdot \mathbf{S} \propto 2(q_z \mathcal{V}_y \sin \phi_y - q_y \mathcal{V}_z \sin \phi_z) e^{2\sqrt{q_y^2 + q_z^2}x} = 0. \quad (3)$$

The modulus $|\mathbf{S}|$ depends on the field amplitudes and excitation power. Equations (1) and (3) fix the chirality index $C_{\mathbf{q}} \equiv (-\hat{\mathbf{x}}) \cdot (\hat{\mathbf{S}} \times \hat{\mathbf{q}})$ as follows. Except for the singular values $\phi_y \neq \{0, \pi/2, \pi, 3\pi/2\}$,

$$\frac{\mathcal{V}_y}{\mathcal{V}_z} = -\frac{q_z \cos \phi_z}{q_y \cos \phi_y} = \frac{q_y \sin \phi_z}{q_z \sin \phi_y} \quad (4)$$

leads to $q_z^2 \tan \phi_y + q_y^2 \tan \phi_z = 0$ and by substitution into Eq. (1) $\mathcal{V}_y e^{i\phi_y} = q_y e^{i\phi_y} / (\sqrt{q_y^2 + q_z^2} \sin \phi_y)$ and $\mathcal{V}_z e^{i\phi_z} = q_z e^{i\phi_z} / (\sqrt{q_y^2 + q_z^2} \sin \phi_z)$, such that

$$C_{\mathbf{q}} = \left[\frac{q_y^2 q_z^2 \sin^2(\phi_y - \phi_z)}{(q_y^2 + q_z^2)^2 \sin^2 \phi_y \sin^2 \phi_z} + 1 \right]^{-1/2} > 0. \quad (5)$$

Hence, any source-free evanescent vector field with transverse spin must be ‘‘right-handed’’, implying the presence of a geometric SOC. Because $0 < |C_{\mathbf{q}}| \leq 1$, the spin cannot be perpendicular to the propagation plane. $C_{\mathbf{q}} = 1$ indicates that the spin lies in the plane with $S_x \rightarrow 0$ and maximizes the chirality index, so the three vectors $\{-\hat{\mathbf{x}}, \hat{\mathbf{S}}, \hat{\mathbf{q}}\}$ are locked into right angles. When $\phi_y = \phi_z \rightarrow \{\pi/2, 3\pi/2\}$, $\mathcal{V}_y e^{i\phi_y} = iq_y / \sqrt{q_y^2 + q_z^2}$, $\mathcal{V}_z e^{i\phi_z} = iq_z / \sqrt{q_y^2 + q_z^2}$, and $\mathcal{V}_y / \mathcal{V}_z = \pm q_y / q_z$. Finally, for $\phi_y = 0$ or π , $\phi_z = 0$ or π , $\sqrt{q_y^2 + q_z^2} = 0$, such that the field is standing.

Stray fields with maximal chirality.—We illustrate the chirality of stray magnetic fields at the hand of a point magnetic moment source $\hat{\mathbf{m}}(t)$, noting that the finite size of the source can easily be incorporated by proper form factors (see below). The arguments equally apply to the electric stray fields of an electric dipole moment with transverse dynamics $\mathbf{p}(t) = p\hat{\mathbf{p}}(t)$.

An in-plane magnetic field \mathbf{H}_0 at an angle θ with the $\hat{\mathbf{z}}$ -axis controls the dot magnetization $\hat{\mathbf{M}}_s$. Here we disregard in-plane anisotropy by assuming $\hat{\mathbf{M}}_s \parallel \mathbf{H}_0$ for simplicity and refer to the Supplemental Material (SM) [50]

for a more general treatment. For convenience, we introduce a local $\{\tilde{x}, \tilde{y}, \tilde{z}\}$ -reference frame with $\tilde{\mathbf{z}} \parallel \hat{\mathbf{M}}_s$ and $\tilde{\mathbf{x}} \parallel \hat{\mathbf{x}} \parallel \hat{\mathbf{n}}$. The dynamic magnetization of the source $\hat{\mathbf{M}}(\mathbf{r}, t) = \delta(\mathbf{r})\hat{\mathbf{m}}(t) = \delta(\mathbf{r})(\delta\tilde{m}e^{-i\Omega t}, i\xi^2\delta\tilde{m}e^{-i\Omega t}, \tilde{m}_s)^T$, where \tilde{m}_s is the saturation magnetic moment, $\delta\tilde{m} \ll \tilde{m}_s$ represents the small transverse fluctuation of magnetic moment, and $\xi^2 > 0$ is the ellipticity of polarization. By rotation to the laboratory $\{x, y, z\}$ -frame, the components of magnetic moment $\tilde{m}_x = \delta\tilde{m}e^{-i\Omega t}$, $\tilde{m}_y = i\xi^2\delta\tilde{m}e^{-i\Omega t} \cos \theta + \tilde{m}_s \sin \theta$, $\tilde{m}_z = -i\xi^2\delta\tilde{m}e^{-i\Omega t} \sin \theta + \tilde{m}_s \cos \theta$. The dipolar field follows from Coulomb’s law $h_{\beta}(\mathbf{r}, t) = 1/(4\pi)\partial_{\beta}\partial_{\alpha}\int_{-\infty}^{\infty} d\mathbf{r}'\tilde{M}_{\alpha}(\mathbf{r}', t)/|\mathbf{r} - \mathbf{r}'| = \sum_{q_y, q_z} e^{i(q_y y + q_z z)} h_{\beta}(x, q_y, q_z)$, in the summation convention over repeated Cartesian indices $\{\alpha, \beta\} = \{x, y, z\}$. For $x < 0$ the Fourier components

$$\begin{aligned} h_x(x, q_y, q_z) &= \mathcal{F}_{q_y, q_z} e^{\sqrt{q_y^2 + q_z^2}x} / 2, \\ h_y(x, q_y, q_z) &= \mathcal{F}_{q_y, q_z} e^{\sqrt{q_y^2 + q_z^2}x} iq_y / (2\sqrt{q_y^2 + q_z^2}), \\ h_z(x, q_y, q_z) &= \mathcal{F}_{q_y, q_z} e^{\sqrt{q_y^2 + q_z^2}x} iq_z / (2\sqrt{q_y^2 + q_z^2}), \end{aligned} \quad (6)$$

where $\mathcal{F}_{q_y, q_z} = \tilde{m}_x \sqrt{q_y^2 + q_z^2} + \tilde{m}_y iq_y + \tilde{m}_z iq_z$. The near field obeys the locking relation $iq_y h_y(x, q_y, q_z) + iq_z h_z(x, q_y, q_z) = -\sqrt{q_y^2 + q_z^2} h_x(x, q_y, q_z)$.

The spin density of the stray magnetic field (6) $\mathbf{S}(x, q_y, q_z) = (\mu_0/4\Omega)\text{Im}[\mathbf{h}^*(x, q_y, q_z) \times \mathbf{h}(x, q_y, q_z)]$ [4, 19, 20, 51, 52]. In the lower half-space ($x < 0$)

$$\begin{aligned} S_x(x, q_y, q_z) &= 0, \\ S_y(x, q_y, q_z) &= -\frac{\mu_0}{8\Omega} |\mathcal{F}_{q_y, q_z}|^2 q_z e^{2\sqrt{q_y^2 + q_z^2}x} / \sqrt{q_y^2 + q_z^2}, \\ S_z(x, q_y, q_z) &= \frac{\mu_0}{8\Omega} |\mathcal{F}_{q_y, q_z}|^2 q_y e^{2\sqrt{q_y^2 + q_z^2}x} / \sqrt{q_y^2 + q_z^2}. \end{aligned} \quad (7)$$

The field is perfectly spin-momentum locked with $C_{\mathbf{q}} = 1$ and therefore an example for Eq. (5) with fixed phase $\phi_y = \phi_z = \pi/2$ and spin \mathbf{S} lying in the propagation plane. The Rashba SOC of free electrons obeys the same relation, *viz.* $\mathbf{q} \cdot \mathbf{S} = 0$ with integer chirality $\hat{\mathbf{n}} \cdot (\hat{\mathbf{S}} \times \hat{\mathbf{q}}) = 1$. The spin density $\mathbf{S}(x, \mathbf{q})$ is maximized at $\mathbf{q} = (-1/x, \pi - \theta)$ in the polar coordinate. Figure 2 shows plots of the spin density \mathbf{S} as a function of the wave numbers q_y and q_z when $\xi^2 = 3.3$, referring to the parameters in Fig. 3(a)-(c) below. It indicates that the chirality of the dipolar field is always ‘‘right-handed’’. Below we illustrate other consequences of the photonic SOC.

Steering magnon flow by photonic SOC.—The spin-momentum locking of stray field becomes apparent when interacting with other quasi-particles, such as magnons in an underlying magnet. We consider here an ultra-thin and soft magnetic film of thickness s excited by a magnetic disk of radius w and thickness d while examining the anisotropic cases in the SM [50]. An optional thin insulating spacer between the point source

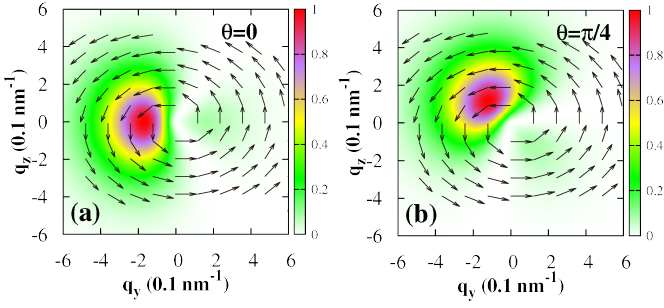


FIG. 2. Spin density \mathbf{S} of the evanescent magnetic fields emitted by a point source at a distance $x = -6$ nm as a function of in-plane wave numbers q_y and q_z and different directions of the in-plane applied magnetic field $\theta = \{0, \pi/4\}$. The arrows represent the direction and the colors the modulus $|\mathbf{S}|$. An analytic estimate of the wave number maximizing $|\mathbf{S}|$ in polar coordinates is $\mathbf{q}_{\max} = (-1/x, \pi - \theta)$. Here $-1/x = 0.17 \text{ nm}^{-1}$ agrees with the numerical results.

and magnetic substrate may suppress the interfacial exchange interaction while leaving their long-ranged dipolar interaction unaffected [14, 53]. Without crystal and shape anisotropies, the equilibrium magnetizations and the in-plane magnetic field H_0 applied at an angle θ are parallel. In thin films the lowest perpendicular standing spin wave dispersion (without small dipolar corrections) $\omega(k) = \mu_0\gamma(H_0 + \alpha_{\text{ex}}M_s k^2)$, where α_{ex} is the exchange stiffness of the film and γ is the modulus of the electron gyromagnetic ratio, lies well below the higher subbands. Retaining the lowest term of Holstein-Primakoff expansion [54, 55] of the spin operator $\hat{\mathbf{S}}$, the magnetization operator $\hat{\mathbf{M}} = -\gamma\hbar\hat{\mathbf{S}}$ of the film

$$\begin{aligned}\hat{M}_y(\boldsymbol{\rho}) &= M_s \sin \theta - \sqrt{2M_s\gamma\hbar} \sum_{\mathbf{k}} (\mathcal{M}_y e^{i\mathbf{k}\cdot\boldsymbol{\rho}} \hat{m}_{\mathbf{k}} + \text{h.c.}) \cos \theta, \\ \hat{M}_z(\boldsymbol{\rho}) &= M_s \cos \theta + \sqrt{2M_s\gamma\hbar} \sum_{\mathbf{k}} (\mathcal{M}_y e^{i\mathbf{k}\cdot\boldsymbol{\rho}} \hat{m}_{\mathbf{k}} + \text{h.c.}) \sin \theta, \\ \hat{M}_x(\boldsymbol{\rho}) &= -\sqrt{2M_s\gamma\hbar} \sum_{\mathbf{k}} (\mathcal{M}_x e^{i\mathbf{k}\cdot\boldsymbol{\rho}} \hat{m}_{\mathbf{k}} + \text{h.c.}),\end{aligned}\quad (8)$$

where the in-plane position vector $\boldsymbol{\rho} = y\hat{\mathbf{y}} + z\hat{\mathbf{z}}$ and $\hat{m}_{\mathbf{k}}$ annihilates a magnon with wave vector \mathbf{k} . For circular polarization $\mathcal{M}_x = -1/(2\sqrt{L_y L_z s})$ and $\mathcal{M}_y = -i/(2\sqrt{L_y L_z s})$ [56]. $\hat{m}_{\mathbf{k}}$ interacts with the stray field of a Kittel magnon $\hat{\beta}$ of nanomagnet by Zeeman interaction [57] $\hat{H}_c = -\mu_0 \int_{-s}^0 dx \int_{-\infty}^{\infty} dy dz \hat{\mathbf{h}}(\mathbf{r}) \cdot \hat{\mathbf{M}}(\mathbf{r}) = \sum_{\mathbf{k}} \hbar g_{\mathbf{k}} \hat{m}_{\mathbf{k}} \hat{\beta}^\dagger + \text{h.c.}$, with coupling constant

$$\begin{aligned}g_{\mathbf{k}} &= -4\pi\mu_0\gamma w \sqrt{M_s \tilde{M}_s} (1 - e^{-kd}) (1 - e^{-ks}) J_1(kw) \\ &\times \frac{1}{k^4} (\mathcal{M}_x, \mathcal{M}_y) \begin{pmatrix} k^2 & -ik\kappa \\ -ik\kappa & -\kappa^2 \end{pmatrix} \begin{pmatrix} \tilde{\mathcal{M}}_x^* \\ \tilde{\mathcal{M}}_y^* \end{pmatrix},\end{aligned}$$

where $J_1(x)$ is the first-order Bessel function of the first kind, $\kappa = k_y \cos \theta - k_z \sin \theta$, $\tilde{\mathcal{M}}_{\tilde{x}} = -1/(2\xi\sqrt{\pi w^2 d})$

and $\tilde{\mathcal{M}}_{\tilde{y}} = -i\xi/(2\sqrt{\pi w^2 d})$ are the amplitudes of Kittel modes in the nanomagnet, and the ellipticity $\xi^2 = \sqrt{(H_0 + (N_{\perp} - N_{\parallel})\tilde{M}_s)/H_0}$ with demagnetization factors $N_{\parallel} \simeq d/(2d + \sqrt{\pi}w)$ and $N_{\perp} \simeq \sqrt{\pi}w/(2d + \sqrt{\pi}w)$ [58].

The associated quantum Langevin equation of motion [59, 60] $id\hat{m}_{\mathbf{k}}/dt = (\omega_{\mathbf{k}} - i\delta_m)\hat{m}_{\mathbf{k}} + g_{\mathbf{k}}\hat{\beta}$ and $id\hat{\beta}/dt = (\Omega - i\delta_{\beta})\hat{\beta} + \sum_{\mathbf{k}} g_{\mathbf{k}}\hat{m}_{\mathbf{k}}$, in which $\Omega = \mu_0\gamma\sqrt{H_0(H_0 + (N_{\perp} - N_{\parallel})\tilde{M}_s)}$ lies in the continuum of $\omega_{\mathbf{k}}$, $\delta_{\beta} = \tilde{\alpha}_G\Omega$, and $\delta_m = \alpha_G\omega_{\mathbf{k}}$ with $\tilde{\alpha}_G$ and α_G denoting, respectively, the damping constants of the nanomagnets and film. Exciting the nanomagnet resonantly by microwaves of frequency Ω to an amplitude $\langle\hat{\beta}(\omega)\rangle$, $\langle\hat{m}_{\mathbf{k}}(\omega)\rangle = g_{\mathbf{k}}\langle\hat{\beta}(\omega)\rangle/(\Omega - \omega_{\mathbf{k}} + i\delta_m)$. Substituting into Eq. (8), we obtain the excited magnetization in the film,

$$\begin{aligned}\langle\hat{M}_x(\boldsymbol{\rho})\rangle &= -\sqrt{2M_s\gamma\hbar} \left(\mathcal{M}_x G(\boldsymbol{\rho}) \langle\hat{\beta}\rangle + \text{h.c.} \right), \\ \langle\hat{M}_y(\boldsymbol{\rho})\rangle &= -\sqrt{2M_s\gamma\hbar} \left(\mathcal{M}_y G(\boldsymbol{\rho}) \langle\hat{\beta}\rangle + \text{h.c.} \right) \cos \theta, \\ \langle\hat{M}_z(\boldsymbol{\rho})\rangle &= \sqrt{2M_s\gamma\hbar} \left(\mathcal{M}_y G(\boldsymbol{\rho}) \langle\hat{\beta}\rangle + \text{h.c.} \right) \sin \theta,\end{aligned}\quad (9)$$

where the Green function

$$\begin{aligned}G(\boldsymbol{\rho}) &= \sum_{\mathbf{k}} e^{i\mathbf{k}\cdot\boldsymbol{\rho}} \frac{g_{\mathbf{k}}}{\Omega - \omega_{\mathbf{k}} + i\delta_m} = -i \frac{L_y L_z}{4\pi} \\ &\times \begin{cases} \int_0^{2\pi} d\varphi (k_{\Omega}/v_{k_{\Omega}}) g(k_{\Omega}, \varphi), & \rho = 0 \\ \int_{\phi-\pi/2}^{\phi+\pi/2} d\varphi (2k_{\Omega}/v_{k_{\Omega}}) g(k_{\Omega}, \varphi) e^{iq_{\Omega}\rho \cos(\varphi-\phi)}, & \rho \neq 0 \end{cases}.\end{aligned}$$

Here $k_{\Omega} = \sqrt{(\Omega - \mu_0\gamma H_0)/(\mu_0\gamma\alpha_{\text{ex}}M_s)}$ is a resonant wave number, $q_{\Omega} = k_{\Omega}(1 + i\alpha_G/2)$, and in polar coordinates $\boldsymbol{\rho} = \{\rho, \phi\}$.

Figure 3(a) plots the directional coupling constant $g_{\mathbf{k}}$. Figure 3(b) and (c) plots the excited magnetization texture in a thin yttrium iron garnet (YIG) film of $s = 10$ nm below the CoFeB disk with dimensions $\{w, d\} = \{300, 50\}$ nm and excitation amplitude $\langle\hat{\beta}\rangle = 1 \times 10^6$ or $M_x/M_s \approx 0.03$, where $\mu_0 M_s = 0.177$ T [35], the exchange stiffness $\alpha_{\text{ex}} = 3 \times 10^{-16} \text{ m}^2$ [35], the Gilbert damping constant $\alpha_G = 10^{-4}$, $\gamma = 1.82 \times 10^{11} \text{ s}^{-1} \cdot \text{T}^{-1}$, and $\mu_0 \tilde{M}_s = 1.6$ T [61]. We find a strongly anisotropic “lighthouse” distribution of the emitted magnons, i.e., narrow beams that can be steered by the direction of YIG’s (soft) equilibrium magnetization, governed by the photonic SOC (Fig. 2). While the spin wave caustics excited by microwave striplines reflect the anisotropy of the spin-wave dispersion in thicker films [62], the point source causes the surprising star-like features here. Diamond NV-center microscopy is the method of choice to confirm our predictions [62].

Figure 3(d) shows the magnetization dynamics when Ω lies below the spin-wave continuum for the parameters also used in Fig. 4 below. The chirality is suppressed when Ω lies below the magnon band $\omega_{\mathbf{k}}$ because only then the Green function $G(-\boldsymbol{\rho}) =$

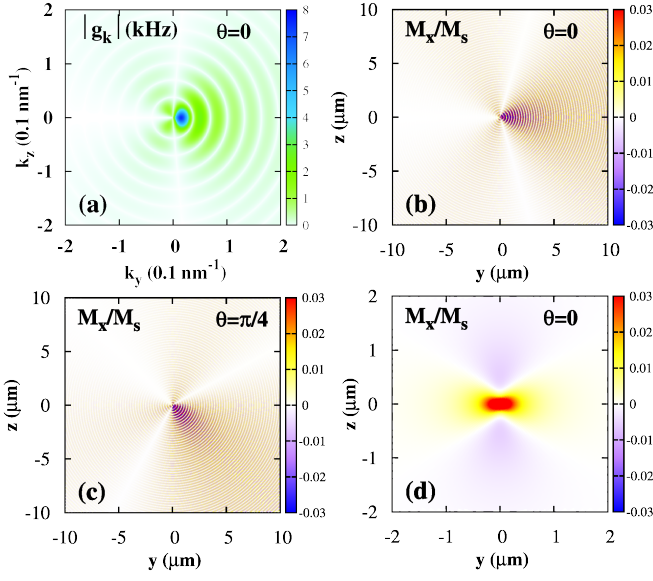


FIG. 3. Magnetization dynamics of a thin magnetic film excited by a magnetic disc under FMR with frequency Ω , cf. Fig. 1. (a) is the coupling constant $g_{\mathbf{k}}$. (b) and (c) show the routing of resonantly excited spin waves with $\Omega > \omega_{\mathbf{k}}$. Since disc and film are assumed to be magnetically soft, a variation of the magnetic field direction $\theta = \{0, \pi/4\}$ rigidly rotates the magnetization distribution. (d) illustrates the magnetization dynamics under non-resonant microwave excitation $\Omega < \omega_{\mathbf{k}}$. The parameters are given in the text.

$\sum_{\mathbf{k}} e^{-i\mathbf{k}\cdot\boldsymbol{\rho}} g_{\mathbf{k}} / (\Omega - \omega_{\mathbf{k}} + i\delta_m) \approx G(\boldsymbol{\rho})^*$ since the intrinsic δ_m in the denominator is small and $\langle \hat{M}_x(\boldsymbol{\rho}) \rangle = -\sqrt{2M_s\gamma\hbar} (\mathcal{M}_x G(\boldsymbol{\rho}) \langle \hat{\beta} \rangle + \text{h.c.}) = \langle \hat{M}_x(-\boldsymbol{\rho}) \rangle$. A larger detuning decreases the exponential decay length of the virtually excited spin waves.

Routing on-chip spin information.—Long-distance entanglement [63] enables the scalability of quantum processors [64]. Magnons are currently under intense investigation, in theory [65–69] and experiment [70], but primarily in one-dimensional systems. Here, we demonstrate that magnons excited by a local source in two-dimensional magnetic film enable an on-chip controllable and long-distance coherent coupling of spin information stored in two distant nanomagnets. For quantum applications, diamond NV-centers [65, 69, 71] have advantages over nanomagnets, representing a qubit with low damping. Reference [70] reports coupling of NV-centers by magnon exchange. However, control of single NV centers in the form of distance to the film and spin direction is difficult, and the coupling strength is weak. Here we focus on a pair of nanostructured magnets that can be fabricated and controlled relatively easily in a single device with a much stronger coupling.

We illustrate the physics at the hand of two identical nanomagnets at a distance ρ_0 on top of the magnetic film at $(y, z) = (-\rho_0/2, 0)$ and $(\rho_0/2, 0)$, as illustrated in

Fig. 4(a). The magnetic field and all the magnetizations point in the same direction. In contrast to the “magnon trap” [72] in which we considered the dissipative regime of exciting real spin waves, we focus here on resonance frequencies Ω below the magnon band gap. We can then trace out the virtual magnons in the film to obtain an effective interaction Hamiltonian between the two disks

$$\mathcal{H}_{\text{eff}} = \hbar \hat{\mathcal{M}}^\dagger \begin{pmatrix} \Omega + \Gamma_{11} & \Gamma_{12} \\ \Gamma_{21} & \Omega + \Gamma_{22} \end{pmatrix} \hat{\mathcal{M}},$$

where $\hat{\mathcal{M}} \equiv (\hat{\beta}_1, \hat{\beta}_2)^T$ are magnon operators of two nanomagnets. The virtual magnons in the films push down the nanomagnet FMR frequencies by $\Gamma_{11} = \Gamma_{22} = \sum_{\mathbf{k}} |g(\mathbf{k}, \theta)|^2 / (\Omega - \tilde{\omega}_{\mathbf{k}})$, and induce an effective coherent coupling $\Gamma_{12}(\rho_0, \theta) = \Gamma_{21}^* = \sum_{\mathbf{k}} |g(\mathbf{k}, \theta)|^2 e^{i\mathbf{k}\cdot\boldsymbol{\rho}_0} / (\Omega - \tilde{\omega}_{\mathbf{k}})$, where $\tilde{\omega}_{\mathbf{k}} = \mu_0\gamma(H_0 + \alpha_{\text{ex}}M_s k^2)(1 - i\alpha_G)$ and we introduced the damping constant α_G of the film and assume that the damping in the nanomagnet is negligibly small.

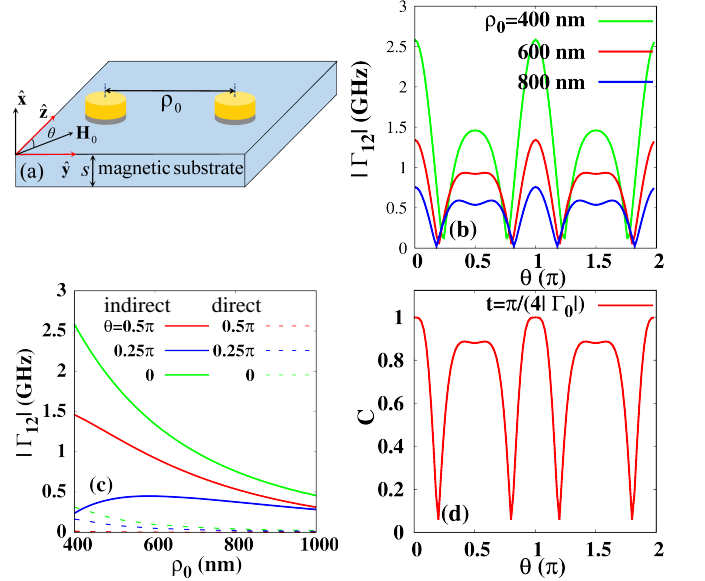


FIG. 4. Coupling and entanglement of two nanomagnets mediated by spin waves in a magnetic film. (a) illustrates the configuration. (b) shows the magnetization direction dependence of the coupling constant Γ_{12} at $\rho_0 = \{400, 600, 800\}$ nm. (c) compares the indirect (solid curve) and direct (dashed curve) interactions as a function of the distance between nanomagnets for different magnetization directions. (d) shows a density plot of the entanglement as a function of θ with fixed time $t = \pi/(4|\Gamma_0|)$ at $\rho_0 = 600$ nm, where $|\Gamma_0|$ is the maximal value of the coupling Γ_{12} .

Figure 4(b) illustrates the dependence of Γ_{12} on the angle of an applied field with strength $\mu_0 H_0 = 0.1$ T at constant distance between two equal YIG disks of dimensions $\{w, d\} = \{100, 180\}$ nm on top of a thin CoFeB film of thickness $s = 10$ nm, which is of long-range and much larger than the direct dipolar interaction (refer to the

SM [50]) [Fig. 4(c)]. We chose here the material combination from Fig. 3(d) to ensure that the magnon frequencies lie above that of the nanomagnet FMR to ensure the virtual exchange of magnons.

The exchange stiffness of CoFeB $\alpha_{\text{ex}} = 8 \times 10^{-17} \text{ m}^2$ [73, 74] and its Gilbert damping constant $\alpha_G = 10^{-3}$ [75]. The magnon band of a film with $\mu_0 M_s = 1.6 \text{ T}$ [61] $\omega(\mathbf{k}) \geq \mu_0 \gamma \sqrt{H_0(H_0 + M_s)} > \mu_0 \gamma H_0 = 18.2 \text{ GHz} > \Omega = 18.1 \text{ GHz}$ lies above the FMR frequency of the disks. Even though the chirality vanishes in the virtual excitation [see Fig. 3(d)] the coupling Γ_{12} is still strongly angle-dependent, with maxima in the GHz regime at $\theta = \{0, \pi\}$ with large cooperativities [76] $\mathcal{C} = 4|\Gamma_{12}|^2/(\tilde{\alpha}_G \Omega)^2 \sim 10^6$. The photonic SOC forbids magnon exchange for angles $\theta = \{\pi/4, 3\pi/4\}$ at which the coupling nearly vanishes.

The anisotropic indirect coupling Γ_{12} generates a tunable entanglement between two distant nanomagnets, as in Fig. 4(d). We now consider the quantum dynamics of the system initialized to a state with a single magnon in one nanomagnet denoted as $|1, 0\rangle$. The quantum dynamics of the two nanomagnets obey the quantum master equation for the density matrix ρ at zero temperature $d\rho/dt = -(i/\hbar)[\mathcal{H}_{\text{eff}}, \rho] + \delta_\beta \mathcal{L}[\beta_1] + \delta_\beta \mathcal{L}[\beta_2]$, where the Lindblad dissipation operator $\mathcal{L}[\beta] \equiv \beta \rho \beta^\dagger - \{\beta^\dagger \beta, \rho\}/2$ represents the magnon damping. The concurrence [49, 77, 78] $C(t, \theta) = 2|\rho_{12}| = e^{-\delta_\beta t} |\sin[2\Gamma_{12}(\theta)t]|$ is a useful measure of the time-dependent entanglement of the magnon states. At a fixed angle θ , the concurrence is maximal for $t_0 \equiv \pi/(4|\Gamma_{12}|)$, at which the two nanomagnets form a fully delocalized Bell-state $|\varphi\rangle = (|1, 0\rangle - i|0, 1\rangle)/\sqrt{2}$ with fidelity: $\mathcal{F} = \text{Tr}[\rho(t_0)|\varphi\rangle\langle\varphi|] = \exp[-\pi\tilde{\alpha}_G\Omega/(4|\Gamma_{12}|)] \rightarrow 1$.

Conclusion.—To conclude, we report a geometric SOC of magnetic stray fields in two dimensions, viz. the spin of a near-field evanescent normal to a plane of propagation is always normal to its wave vector, and the associated chirality is always right-handed. In nanomagnetic structures on top of ultrathin magnetic films this leads to a routed excitation of magnons that may tune the strong coupling between two or more nanomagnets by the magnetization directions to high cooperativities, thereby facilitating scalable magnon-based classical or quantum information processors. The next step is entangling a two-dimensional lattice of magnetic dots (magnonic crystal) that can provide more options to control quantum information.

This work is financially supported by the National Key Research and Development Program of China under Grant No. 2023YFA1406600, the National Natural Science Foundation of China under Grant No. 12374109, and the startup grant of Huazhong University of Science and Technology. J.Z. acknowledges the support of the Georg H. Endress Foundation. The JSPS KAKENHI Grants No. 19H00645, 22H04965, and JP24H02231 support G.B. financially. We thank Mehrdad Elyasi for illu-

minating discussions.

* These authors contributed equally to this work.

† taoyuphy@hust.edu.cn

- [1] L. Novotny and B. Hecht, *Principles of Nano-Optics* (Cambridge University Press, Cambridge, England, 2006).
- [2] F. J. Rodríguez-Fortuño, G. Marino, P. Ginzburg, D. O'Connor, A. Martínez, G. A. Wurtz, and A. V. Zayats, Near-Field Interference for the Unidirectional Excitation of Electromagnetic Guided Modes, *Science* **340**, 328 (2013).
- [3] P. Lodahl, S. Mahmoodian, S. Stobbe, A. Rauschenbeutel, P. Schneeweiss, J. Volz, H. Pichler, and P. Zoller, Chiral quantum optics, *Nature* **541**, 473 (2017).
- [4] K. Y. Bliokh and F. Nori, Transverse and longitudinal angular momenta of light, *Phys. Rep.* **592**, 1 (2015).
- [5] K. Y. Bliokh, D. Smirnova, and F. Nori, Quantum spin Hall effect of light, *Science* **348**, 1448 (2015).
- [6] B. Lenk, H. Ulrichs, F. Garbs, and M. Münzenberg, The building blocks of magnonics, *Phys. Rep.* **507**, 107 (2011).
- [7] A. V. Chumak, V. I. Vasyuchka, A. A. Serga, and B. Hillebrands, Magnon spintronics, *Nat. Phys.* **11**, 453 (2015).
- [8] D. Grundler, Nanomagnonics around the corner, *Nat. Nanotech.* **11**, 407 (2016).
- [9] V. E. Demidov, S. Urazhdin, G. de Loubens, O. Klein, V. Cros, A. Anane, and S. O. Demokritov, Magnetization oscillations and waves driven by pure spin currents, *Phys. Rep.* **673**, 1 (2017).
- [10] A. Brataas, B. van Wees, O. Klein, G. de Loubens, and M. Viret, Spin Insulatronics, *Phys. Rep.* **885**, 1 (2020).
- [11] A. Barman, G. Gubbiotti, S. Ladak, A. O. Adeyeye, M. Krawczyk, J. Gräfe, C. Adelman, S. Cotofana, A. Naeemi, V. I. Vasyuchka *et al.*, The 2021 magnonics roadmap, *J. Phys. Condens. Matter.* **33**, 413001 (2021).
- [12] B. Flebus, S. Rezende, D. Grundler, and A. Barman, Recent advances in magnonics, *J. Appl. Phys.* **133**, 160401 (2023).
- [13] K. Baumgaertl and D. Grundler, Reversal of nanomagnets by propagating magnons in ferrimagnetic yttrium iron garnet enabling nonvolatile magnon memory, *Nat. Commun.* **14**, 1490 (2023).
- [14] A. Mucchietto, K. Baumgaertl, and D. Grundler, Magnon-assisted magnetization reversal of $\text{Ni}_{81}\text{Fe}_{19}$ nanostripes on $\text{Y}_3\text{Fe}_5\text{O}_{12}$ with different interfaces, *ACS Nano* **18**, 8641 (2024).
- [15] D. L. Quirion, Y. Tabuchi, S. Ishino, A. Noguchi, T. Ishikawa, R. Yamazaki, and Y. Nakamura, Resolving quanta of collective spin excitations in a millimeter-sized ferromagnet, *Sci. Adv.* **3**, e1603150 (2017).
- [16] D. Xu, X. K. Gu, H. K. Li, Y. C. Weng, Y. P. Wang, J. Li, H. Wang, S. Y. Zhu, and J. Q. You, Quantum control of a single magnon in a macroscopic spin system, *Phys. Rev. Lett.* **130**, 193603 (2023).
- [17] Y. Tabuchi, S. Ishino, A. Noguchi, T. Ishikawa, R. Yamazaki, K. Usami, and Y. Nakamura, Coherent coupling between a ferromagnetic magnon and a superconducting qubit, *Science* **349**, 405 (2015).

- [18] D. L. Quirion, S. P. Wolski, Y. Tabuchi, S. Kono, K. Usami, and Y. Nakamura, Entanglement-based single-shot detection of a single magnon with a superconducting qubit, *Science* **367**, 425 (2020).
- [19] R. W. Damon and J. R. Eshbach, Magnetostatic modes of a ferromagnet slab, *J. Phys. Chem. Solids* **19**, 308 (1961).
- [20] L. R. Walker, Magnetostatic modes in ferromagnetic resonance, *Phys. Rev.* **105**, 390 (1957).
- [21] T. Yu, Z. C. Luo, and G. E. W. Bauer, Chirality as generalized spin-orbit interaction in spintronics, *Phys. Rep.* **1009**, 1 (2023).
- [22] Z. H. Jiang, J. Lim, Y. Li, W. Pfaff, T.-H. Lo, J. C. Qian, A. Schleife, J.-M. Zuo, V. Novosad, and A. Hoffmann, Integrating magnons for quantum information, *Appl. Phys. Lett.* **123**, 130501 (2023).
- [23] T. Yu, Y. X. Zhang, S. Sharma, X. Zhang, Y. M. Blanter, and G. E. W. Bauer, Magnon Accumulation in Chirally Coupled Magnets, *Phys. Rev. Lett.* **124**, 107202 (2020).
- [24] X. F. Zhang, A. Galda, X. Han, D. F. Jin, and V. M. Vinokur, Broadband Nonreciprocity Enabled by Strong Coupling of Magnons and Microwave Photons, *Phys. Rev. Applied* **13**, 044039 (2020).
- [25] N. Zhu, X. Han, C. L. Zou, M. R. Xu, and H. X. Tang, Magnon-photon strong coupling for tunable microwave circulators, *Phys. Rev. A* **101**, 043842 (2020).
- [26] L. H. Zhong, C. Zhang, and B. M. Yao, Controlling the dynamics of cavity magnon polariton via microwave polarization, *AIP Advances* **12**, 085323 (2022).
- [27] J.-K. Xie, S.-L. Ma, Y.-L. Ren, S.-Y. Gao, and F.-L. Li, Chiral cavity-magnonic system for the unidirectional emission of a tunable squeezed microwave field, *Phys. Rev. A* **108**, 033701 (2023).
- [28] H. P. Zhan, L. H. Sun, and H. T. Tan, Chirality-induced one-way quantum steering between two waveguide-mediated ferrimagnetic microspheres, *Phys. Rev. B* **106**, 104432 (2022).
- [29] J. Bourhill, W. C. Yu, V. Vlaminck, G. E. W. Bauer, G. Ruoso, and V. Castel, Generation of Circulating Cavity Magnon Polaritons, *Phys. Rev. Applied* **19**, 014030 (2023).
- [30] Y. Au, E. Ahmad, O. Dmytriiev, M. Dvornik, T. Davison, and V. V. Kruglyak, Resonant microwave-to-spin-wave transducer, *Appl. Phys. Lett.* **100**, 182404 (2012).
- [31] C. P. Liu, J. L. Chen, T. Liu, F. Heimbach, H. M. Yu, Y. Xiao, J. F. Hu, M. C. Liu, H. C. Chang, T. Stueckler, S. Tu, Y. G. Zhang, Y. Zhang, P. Gao, Z. M. Liao, D. P. Yu, K. Xia, N. Lei, W. S. Zhao, and M. Z. Wu, Long-distance propagation of short-wavelength spin waves, *Nat. Commun.* **9**, 738 (2018).
- [32] Y. Shiota, T. Taniguchi, M. Ishibashi, T. Moriyama, and T. Ono, Tunable Magnon-Magnon Coupling Mediated by Dynamic Dipolar Interaction in Synthetic Antiferromagnets, *Phys. Rev. Lett.* **125**, 017203 (2020).
- [33] M. Ishibashi, Y. Shiota, T. Li, S. Funada, T. Moriyama, and T. Ono, Switchable giant nonreciprocal frequency shift of propagating spin waves in synthetic antiferromagnets, *Sci. Adv.* **6**, eaaz6931 (2020).
- [34] K. Szulc, P. Graczyk, M. Mruczkiewicz, G. Gubbiotti, and M. Krawczyk, Spin-wave diode and circulator based on unidirectional coupling, *Phys. Rev. A* **14**, 034063 (2020).
- [35] H. C. Wang, J. L. Chen, T. Yu, C. P. Liu, C. Y. Guo, H. Jia, S. Liu, K. Shen, T. Liu, J. Y. Zhang, M. A. Cabero, Q. M. Song, S. Tu, L. Flacke, M. Althammer, M. Weiler, M. Z. Wu, X. F. Han, K. Xia, D. P. Yu, G. E. W. Bauer, and H. M. Yu, Nonreciprocal coherent coupling of nanomagnets by exchange spin waves. *Nano Res.* **14**, 2133 (2021).
- [36] J. Zou, S. Bosco, E. Thingstad, J. Klinovaja, and D. Loss, Dissipative Spin-Wave Diode and Nonreciprocal Magnonic Amplifier, *Phys. Rev. Lett.* **132**, 036701 (2024).
- [37] C. Y. Cai, D. M. Kennes, M. A. Sentef, and T. Yu, Edge and corner skin effects of chirally coupled magnons characterized by a topological winding tuple, *Phys. Rev. B* **108**, 174421 (2023).
- [38] T. Yu and G. E. W. Bauer, Noncontact spin pumping by microwave evanescent fields, *Phys. Rev. Lett.* **124**, 236801 (2020).
- [39] T. Yu and G. E. W. Bauer, Efficient Gating of Magnons by Proximity Superconductors, *Phys. Rev. Lett.* **129**, 117201 (2022).
- [40] M. Borst, P. H. Vree, A. Lowther, A. Teepe, S. Kurdi, I. Bertelli, B. G. Simon, Y. M. Blanter, and T. van der Sar, Observation and control of hybrid spin-wave-Meissner-current transport modes, *Science* **382**, 430 (2023).
- [41] C. Y. Cai, X. H. Zhou, W. C. Yu, and T. Yu, Acoustic frequency multiplication and pure second-harmonic generation of phonons by magnetic transducers, *Phys. Rev. B* **107**, L100410 (2023).
- [42] M. R. Xu, K. Yamamoto, J. Puebla, K. Baumgaertl, B. Rana, K. Miura, H. Takahashi, D. Grundler, S. Maekawa, and Y. Otani, Nonreciprocal surface acoustic wave propagation via magneto-rotation coupling, *Sci. Adv.* **6**, eabb1724 (2020).
- [43] R. Sasaki, Y. Nii, and Y. Onose, Magnetization control by angular momentum transfer from surface acoustic wave to ferromagnetic spin moments, *Nat. Commun.* **12**, 2599 (2021).
- [44] S. Tateno and Y. Nozaki, Highly nonreciprocal spin waves excited by magnetoelastic coupling in a Ni/Si bilayer, *Phys. Rev. A* **13**, 034074 (2020).
- [45] P. J. Shah, D. A. Bas, I. Lisenkov, A. Matyushov, N. Sun, and M. R. Page, Giant nonreciprocity of surface acoustic waves enabled by the magnetoelastic interaction, *Sci. Adv.* **6**, eabc5648 (2020).
- [46] D. A. Bas, R. Verba, P. J. Shah, S. Leontsev, A. Matyushov, M. J. Newburger, N. X. Sun, V. Tyberkevich, A. Slavin, and M. R. Page, Nonreciprocity of phase accumulation and propagation losses of surface acoustic waves in hybrid magnetoelastic heterostructures, *Phys. Rev. A* **18**, 044003 (2022).
- [47] Y. L. Ren, S. L. Ma, and F. L. Li, Chiral coupling between a ferromagnetic magnon and a superconducting qubit, *Phys. Rev. A* **106**, 053714 (2022).
- [48] W. K. Wootters, Entanglement of Formation of an Arbitrary State of Two Qubits, *Phys. Rev. Lett.* **80**, 2245(1998).
- [49] S. A. Hill and W. K. Wootters, Entanglement of a Pair of Quantum Bits, *Phys. Rev. Lett.* **78**, 5022 (1997).
- [50] See Supplemental Material [...] for the calculation of direct dipolar coupling between nanomagnets and photonic spin-orbit coupling of the stray field of anisotropic nanomagnet and its magnon routing in the underlying magnetic film.
- [51] G. S. Kino, *Acoustic Waves: Devices, Imaging, And Analog Signal Processing* (Prentice-Hall, New Jersey, 1987).

- [52] I. A. Viktorov, *Rayleigh and Lamb waves: Physical theory and applications* (Plenum Press, New York, 1967).
- [53] J. L. Chen, C. P. Liu, T. Liu, Y. Xiao, K. Xia, G. E. W. Bauer, M. Z. Wu, and H. M. Yu, Strong interlayer magnon-magnon coupling in magnetic metal-insulator hybrid nanostructures, *Phys. Rev. Lett.* **120**, 217202 (2018).
- [54] T. Holstein and H. Primakoff, Field Dependence of the Intrinsic Domain Magnetization of a Ferromagnet, *Phys. Rev.* **58**, 1098 (1940).
- [55] C. Kittel, *Quantum Theory of Solids* (Wiley, New York, 1963).
- [56] S. Sharma, Y. M. Blanter, and G. E. W. Bauer, Light scattering by magnons in whispering gallery mode cavities, *Phys. Rev. B* **96**, 094412 (2017).
- [57] C. Kittel, On the Theory of Ferromagnetic Resonance Absorption, *Phys. Rev.* **73**, 155 (1948).
- [58] M. Sato and Y. Ishii, Simple and approximate expressions of demagnetizing factors of uniformly magnetized rectangular rod and cylinder, *J. Appl. Phys.* **66**, 983 (1989).
- [59] C. W. Gardiner and M. J. Collett, Input and output in damped quantum systems: Quantum stochastic differential equations and the master equation, *Phys. Rev. A* **31**, 3761 (1985).
- [60] A. A. Clerk, M. H. Devoret, S. M. Girvin, F. Marquardt, and R. J. Schoelkopf, Introduction to quantum noise, measurement, and amplification, *Rev. Mod. Phys.* **82**, 1155 (2010).
- [61] M. Küß, M. Heigl, L. Flacke, A. Hörner, M. Weiler, M. Albrecht, and A. Wixforth, Nonreciprocal Dzyaloshinskii-Moriya Magnetoacoustic Waves, *Phys. Rev. Lett.* **125**, 217203 (2020).
- [62] I. Bertelli, J. J. Carmiggelt, T. Yu, B. G. Simon, C. C. Pothoven, G. E. W. Bauer, Y. M. Blanter, J. Aarts, and T. van der Sar, Magnetic resonance imaging of spin-wave transport and interference in a magnetic insulator, *Sci. Adv.* **6**, eabd3556 (2020).
- [63] A. Einstein, B. Podolsky, and N. Rosen, Can Quantum-Mechanical Description of Physical Reality Be Considered Complete?, *Phys. Rev.* **47**, 777 (1935).
- [64] L. M. K. Vandersypen, H. Bluhm, J. S. Clarke, A. S. Dzurak, R. Ishihara, A. Morello, D. J. Reilly, L. R. Schreiber and M. Veldhorst, Interfacing spin qubits in quantum dots and donors—hot, dense, and coherent, *npj Quantum Inf.* **3**, 34 (2017).
- [65] M. Fukami, D. R. Candido, D. D. Awschalom, and M. E. Flatté, Opportunities for Long-Range Magnon-Mediated Entanglement of Spin Qubits via On- and Off-Resonant Coupling, *PRX Quantum* **2**, 040314 (2021).
- [66] T. Neuman, D. S. Wang, and P. Narang, Nanomagnonic Cavities for Strong Spin-Magnon Coupling and Magnon-Mediated Spin-Spin Interactions, *Phys. Rev. Lett.* **125**, 247702 (2020).
- [67] B. Flebus and Y. Tserkovnyak, Entangling distant spin qubits via a magnetic domain wall, *Phys. Rev. B* **99**, 140403(R) (2019).
- [68] L. Trifunovic, O. Dial, M. Trif, J. R. Wootton, R. Abebe, A. Yacoby, and D. Loss, Long-Distance Spin-Spin Coupling via Floating Gates, *Phys. Rev. X* **2**, 011006 (2012).
- [69] L. Trifunovic, F. L. Pedrocchi, and D. Loss, Long-Distance Entanglement of Spin Qubits via Ferromagnet, *Phys. Rev. X* **3**, 041023 (2013).
- [70] M. Fukami, J. C. Marcks, D. R. Candido, L. R. Weiss, B. Soloway, S. E. Sullivan, N. Deegan, F. J. Heremans, M. E. Flatté, and D. D. Awschalom, Magnon-mediated qubit coupling determined via dissipation measurements, *Proc. Natl. Acad. Sci.* **121**, e2313754120 (2024).
- [71] D. R. Candido, G. D. Fuchs, E. Johnston-Halperin, and M. E. Flatté, Predicted strong coupling of solid-state spins via a single magnon mode, *Mater. Quantum. Technol.* **1**, 011001 (2021).
- [72] T. Yu, H. C. Wang, M. A. Sentef, H. M. Yu, and G. E. W. Bauer, Magnon trap by chiral spin pumping, *Phys. Rev. B* **102**, 054429 (2020).
- [73] H. A. Mook, J. W. Lynn, and R. M. Nicklow, Temperature Dependence of the Magnetic Excitations in Nickel, *Phys. Rev. Lett.* **30**, 556 (1973).
- [74] M. Pajda, J. Kudrnovský, I. Turek, V. Drchal, and P. Bruno, Ab initio calculations of exchange interactions, spin-wave stiffness constants, and Curie temperatures of Fe, Co, and Ni, *Phys. Rev. B* **64**, 174402 (2001).
- [75] H. J. Qin, R. B. Holländer, L. Flašman, F. Hermann, R. Dreyer, G. Woltersdorf, and S. van Dijken, Nanoscale magnonic Fabry-Pérot resonator for low-loss spin-wave manipulation, *Nat. Commun.* **12**, 2293 (2021).
- [76] B. Z. Rameshti, S. V. Kusminskiy, J. A. Haigh, K. Usami, D. Lachance-Quirion, Y. Nakamura, C.-M. Hu, H. X. Tang, G. E. W. Bauer, and Y. M. Blanter, Cavity magnonics, *Phys. Rep.* **979**, 1 (2022).
- [77] J. Zou, S. Zhang, and Y. Tserkovnyak, Bell-state generation for spin qubits via dissipative coupling, *Phys. Rev. B* **106**, L180406 (2022).
- [78] J. Zou, S. K. Kim, and Y. Tserkovnyak, Tuning entanglement by squeezing magnons in anisotropic magnets, *Phys. Rev. B* **101**, 014416 (2020).